

Review

Open Access



New trends in additive manufacturing of high-entropy alloys and alloy design by machine learning: from single-phase to multiphase systems

Yinghao Zhou^{1,2}, Zehuan Zhang³, Dawei Wang⁴, Weicheng Xiao^{1,2}, Jiang Ju^{1,2}, Shaofei Liu^{1,2}, Bo Xiao^{1,2}, Ming Yan⁴, Tao Yang^{1,5*} 

¹Department of Materials Science and Engineering, City University of Hong Kong, Hong Kong, China.

²Centre for Advanced Nuclear Safety and Sustainable Development, City University of Hong Kong, Hong Kong, China.

³College of Physics, Sichuan University, Chengdu 610064, Sichuan, China.

⁴Department of Materials Science and Engineering, Shenzhen Key Laboratory for Additive Manufacturing of High-performance Materials, Southern University of Science and Technology, Shenzhen 518055, Guangdong, China.

⁵Hong Kong Institute for Advanced Study, City University of Hong Kong, Hong Kong, China.

* **Correspondence to:** Prof. Tao Yang, Department of Materials Science and Engineering, City University of Hong Kong. Yeung academic building, Tat Chee Avenue Kowloon, Hong Kong, China. E-mail: taoyang6@cityu.edu.hk

How to cite this article: Zhou Y, Zhang Z, Wang D, Xiao W, Ju J, Liu S, Xiao B, Yan M, Yang T. New trends in additive manufacturing of high-entropy alloys and alloy design by machine learning: from single-phase to multiphase systems. *J Mater Inf* 2022;2:18. <https://dx.doi.org/10.20517/jmi.2022.27>

Received: 18 Sep 2022 **First Decision:** 14 Oct 2022 **Revised:** 22 Oct 2022 **Accepted:** 9 Nov 2022 **Published:** 17 Nov 2022

Academic Editors: Xingjun Liu, Wen Chen, Kotiba Hamad, Wei Xiong **Copy Editor:** Ke-Cui Yang **Production Editor:** Ke-Cui Yang

Abstract

Alloys with excellent properties are always in significant demand for meeting the severe conditions of industrial applications. However, the design strategies of traditional alloys based on a single principal element have reached their limits in terms of property optimization. The concept of high-entropy alloys (HEAs) provides a new design strategy based on multicomponent elements, which may overcome the bottleneck problems that exist in traditional alloys. To further maximize the capability of HEAs, a novel additive manufacturing (AM) technique has been utilized to produce HEA components with the desired structures and properties. This review considers a new trend in the AM of HEAs, i.e., from the AM of single-phase HEAs to multiphase HEAs. Although most as-printed single-phase HEAs show superior tensile properties to as-cast ones, their strength is still not satisfactory, especially at elevated temperatures. Thus, multiphase HEAs are developed by introducing hard second phases, such as L₁, BCC, carbides, oxides, nitrides, and so on. These phases can be introduced to the matrix using *in situ* alloying during AM or the subsequent heat treatment. Dislocation strengthening is considered as the main reason



© The Author(s) 2022. **Open Access** This article is licensed under a Creative Commons Attribution 4.0 International License (<https://creativecommons.org/licenses/by/4.0/>), which permits unrestricted use, sharing, adaptation, distribution and reproduction in any medium or format, for any purpose, even commercially, as long as you give appropriate credit to the original author(s) and the source, provide a link to the Creative Commons license, and indicate if changes were made.



for improving the tensile properties of as-printed single-phase HEAs. In contrast, multiple strengthening and toughening mechanisms occur in as-printed multiphase HEAs, which can synergistically enhance their mechanical properties. Furthermore, machine learning provides an effective method to design new alloys with the desired properties and predict the optimal AM parameters for the designed alloys without tedious experiments. The synergistic combination of machine learning and AM will significantly speed up scientific advances and promote industrial applications.

Keywords: High-entropy alloys, additive manufacturing, precipitation hardening, strengthening mechanism, machine learning

INTRODUCTION

High-entropy alloys

High-entropy alloys (HEAs) and multiple-principal element alloys were first proposed by Yeh *et al.* and Cantor *et al.*, respectively, in 2004^[1,2]. Unlike most conventional alloys based on one principal element, this concept provides a new criterion for developing new alloys with five or more principal elements^[3]. The concentration of each principal element generally ranges from 5 to 35 at. %. The properties of HEAs can be modified by changing the type and content of the base elements or by adding some other trace elements. Therefore, various HEAs have been developed with a broad range of microstructure and properties, such as single-phase HEAs (face-centered-cubic (FCC), body-centered-cubic (BCC), hexagonal-close-packed (HCP) and eutectic HEAs (EHEAs) and precipitation-strengthened HEAs^[4-6]. Single-phase FCC HEAs are mainly based on the transition elements of Fe, Co, Cr, Ni and Mn^[2]. Eutectic HEAs (FCC + BCC) are developed by alloying with other elements, such as Al, Nb and Cu^[7-9]. Single-phase BCC systems are mainly based on some refractory elements, such as V, Nb, Mo, Ta, W, Ti and Hf. It has also been reported that rare-earth elements are strong stabilizers for the formation of HCP-phase HEAs, such as YGdTbDyLu, GdTbDyTmLu and HoDyYGdTb^[10,11].

Compared with traditional alloys, HEAs mainly have the following four unique effects^[12]: (a) high-entropy effect in thermodynamics, which benefits the formation of the single phase; (b) sluggish diffusion effect kinetics caused by multiple principal elements; (c) severe lattice distortion effect induced by the variation in atomic diameter and mixing enthalpy; (d) cocktail effect in properties that can be easily optimized by changing the elements and microstructures. These beneficial effects make HEAs very promising as engineering and functional materials. As an essential criterion for evaluating their engineering applications, the tensile properties of HEAs have been widely studied. [Figure 1](#) summarizes the room-temperature tensile properties of HEAs classified based on their crystal structures. HEAs with a single-phase FCC structure possess superior tensile ductility but suffer from poor yield strength^[13-24]. To improve the tensile strength of single-phase FCC HEAs, the hard BCC phase is introduced to the FCC system by adding Al, Cu, Ti, and so on^[9,22,23,25-28]. He *et al.* illustrated that the BCC phase content increased with increasing Al content, which resulted in high hardness and tensile strength. However, the ductility was sacrificed when the BCC phase exceeded a certain content^[22]. Furthermore, some dual-phase HEAs, such as AlCoCrFeNi_{2,1} and CoCrFeNiNb_x, show excellent wear properties even at elevated temperatures^[29,30]. Single-phase BCC HEAs usually contain refractory elements, such as Ti, Nb, Mo, Ta and Hf. Like β -Ti alloys, these single-phase BCC HEAs show almost negligible work hardening capability, resulting in a poor uniform elongation^[31-37].

It is noteworthy that many single-phase HEAs suffer from insufficient strength, especially at elevated temperatures. Therefore, precipitation-strengthened (PS) HEAs have received extensive attention and research in recent years. As shown in [Figure 1](#), PS HEAs show superior tensile strength and uniform elongation to single-phase and eutectic HEAs^[6,38-47]. Precipitation in HEAs can be generally divided into two

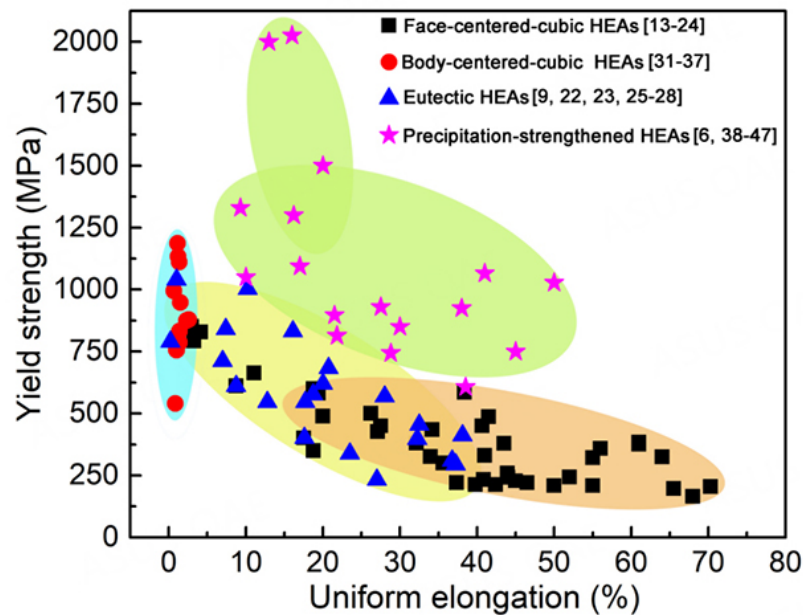


Figure 1. Room-temperature uniaxial tensile properties of HEAs classified based on their phase types: FCC HEAs^[13-24]; BCC HEAs^[31-37]; eutectic HEAs^[9,22,23,25-28]; PS HEAs^[6,38-47]. HEAs: high-entropy alloys.

major categories, namely, coherent and incoherent precipitation. Incoherent precipitation includes the Laves phase (induced by Nb) and topologically close-packed phase (induced by Mo, such as σ and μ phases)^[43,48]. These precipitates significantly improve the strength of HEAs but deteriorate their ductility. The sacrificing of ductility can be attributed to the incoherent interface between the HEA matrix and precipitation, which acts as a source for crack initiation and propagation during deformation. In contrast, the coherent precipitation, i.e., the L_{12} -type phase (γ'), potentially produces a prominent strengthening effect on the matrix without much loss of ductility at cryogenic, room or elevated temperatures. For example, the addition of Ti and Al to FeCoNi can induce a high-content L_{12} phase within the FCC matrix, leading to increases in yield strength from ~ 200 to 1000 MPa, while maintaining a good ductility over 30%^[6]. Furthermore, due to the high-entropy effect, some HEAs decorated by the L_{12} phase exhibit excellent phase stability at elevated temperatures compared with conventional superalloys^[49].

Additive manufacturing

3D printing, formally known as additive manufacturing (AM), has rapidly changed the scenario of future manufacturing by offering significant flexibility for designing and fabricating components with customized structures in a layer-by-layer manner^[50]. AM also provides a flexible method for the *in situ* design of desirable microstructures and properties by controlling the metallurgical behavior within the molten pool^[51,52]. Therefore, this technology shows excellent superiority in fabricating structural and functional materials to conventional processing methods, such as casting, forging and welding.

To date, many kinds of AM technologies, such as fused deposition modeling (FDM), binder jetting (BJ), stereolithography (SLA), digital light projection (DLP), powder bed fusion (PBF) and directed energy deposition (DED), have been developed to fabricate various materials, including polymers, ceramics and metals^[53]. Metallic parts are usually manufactured by the FDM, BJ, PBF and DED AM methods. The FDM and BJ processes use binder materials to glue the metallic powders into products, which subsequently go through multistep heat treatments to remove the binder materials and realize the densification of the parts. Impurities and defects are inevitable for the samples printed by FDM and BJ methods, leading to

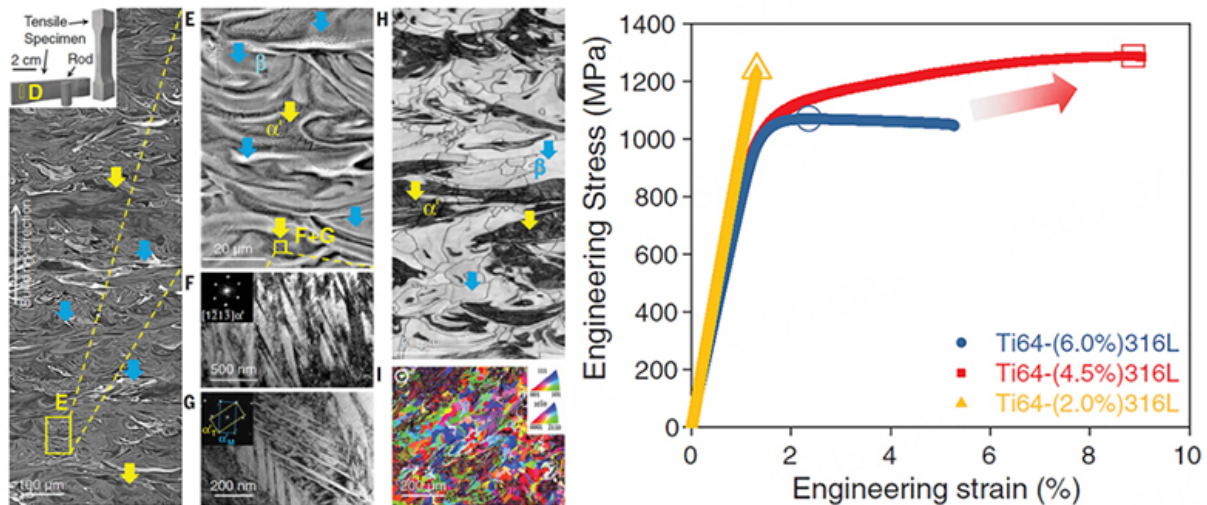


Figure 2. Microstructures with concentration modulation and mechanical properties of as-printed Ti-6Al-4V+(4.5 wt.%) 316L alloy^[52].

unfavorable properties. Compared with the FDM and BJ processes, metallic powders go through sufficient melting and solidification during the PBF and DED processes, leading to near-fully dense parts with excellent properties. PBF processes enable the fabrication of components with high precision by selectively melting a pre-laid powder on an even substrate using a focused high-energy laser beam or electron beam. Unlike PBF processes, DED processes enable the creation of parts on even and uneven substrates by melting the powder or wire using a laser beam, electron beam or electric arc. Therefore, PBF processes are usually used to fabricate the parts with complex structures, while DED processes are usually used to repair engineering and aerospace components. Moreover, DED processes also have significant feasibility in making functionally graded metallic materials^[54].

Both PBF and DED processes undergo ultrafast heating and solidification due to the instantaneous interaction between the high-energy beam and metal powder, which can be considered as nonequilibrium processing^[55]. Therefore, the ultrafine microstructure of the as-printed samples can be obtained, leading to excellent properties^[56]. More importantly, these AM processes provide a unique method to *in situ* design high-performance alloys by changing the compositions and microstructures within the molten pool. For example, Zhang *et al.* *in situ* designed an advanced Ti alloy by doping a small amount of 316L stainless steel to Ti-6Al-4V using laser powder bed fusion (L-PBF), also known as selective laser melting (SLM)^[52]. The micro-concentration modulation was obtained through the partial homogenization of the two alloy melts within the molten pool during L-PBF. As illustrated in Figure 2, the as-printed sample showed a fine scale-modulated $\beta + \alpha'$ dual-phase microstructure, exhibiting a progressive transformation-induced plasticity effect. Therefore, a high tensile strength of ~ 1.3 GPa with a uniform elongation of $\sim 9\%$ and an excellent work-hardening capacity of > 300 MPa was successfully achieved in the as-printed samples. Considering these unique features, PBF and DED processes show significant advantages in making advanced metallic materials with designed microstructures and associated superior properties.

Key issues for HEA design and AM

In recent years, HEAs and AM, as two hot topics, have been extensively studied^[4,57]. However, there are still some key issues that need to be resolved. As mentioned above, the development of single-phase HEAs may have reached a bottleneck in terms of property optimization. Precipitation-strengthened HEAs were therefore designed to break the strength-ductility trade-off of single-phase HEAs. Designing

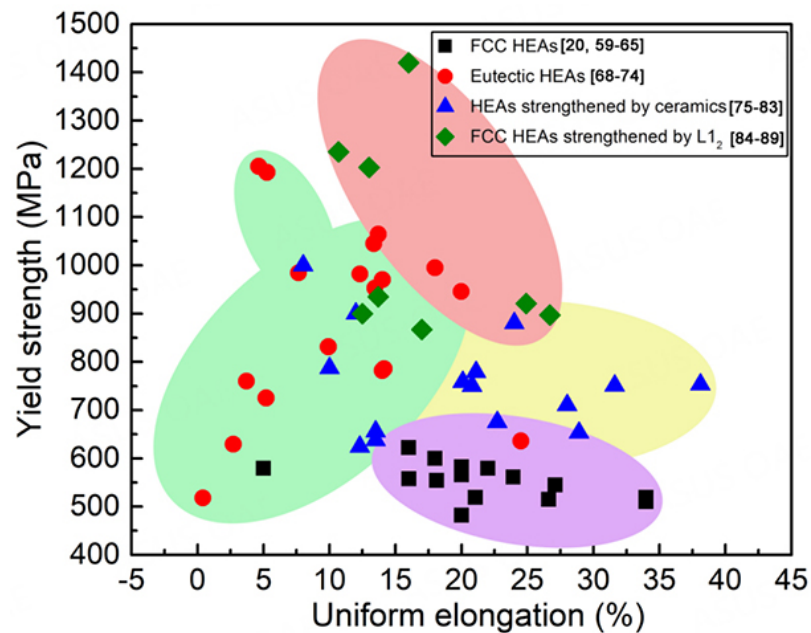


Figure 3. Comparison of tensile yield strength and uniform elongation of various HEAs fabricated by AM: FCC HEAs^[20,59-65]; eutectic HEAs^[68-74]; HEAs strengthened by ceramics^[75-83]; HEAs strengthened by L_{12} ^[84-89]. FCC: face-centered-cubic; HEAs: high-entropy alloys.

precipitation-strengthened HEAs with desirable properties is a significant challenge due to the chemical complexity. Another key issue is the difficulty in obtaining suitable AM processing parameters for these precipitation-strengthened HEAs. Machine learning provides an effective method to quickly screen out alloys with desirable properties and suitable AM processing parameters without tedious experiments^[58]. Thus, this review focuses on some new trends regarding AM precipitation-strengthened HEAs and the applications of machine learning in designing new-type alloys and also obtaining suitable AM processing parameters.

AM OF HEAS

AM processes, including PBF and DED, have shown many significant advantages in fabricating HEA components compared to traditional processing methods, such as casting, wrought and welding. Until now, many kinds of HEAs have been manufactured by AM methods, including single-phase HEAs (FCC or BCC)^[20,59-67], EHEAs (FCC + BCC)^[68-74] and precipitation-strengthened HEAs^[75-89]. Figure 3 summarizes the tensile yield strength against the uniform elongation of as-printed HEAs at room temperature. Due to their poor workability and the high cost of raw materials, only a few studies have been conducted on the AM of BCC HEAs^[66,67]. There is still no report on the tensile properties of BCC HEAs fabricated by AM methods. As-printed FCC HEAs show large ductility but low strength^[20,59-65]. In addition, for EHEAs manufactured by L-PBF, their tensile properties vary over a wide range, which may be caused by the relative proportions between the FCC and BCC phases and different microstructural features^[68-74]. Another approach to strengthening the soft FCC matrix is to introduce second hardening phases, such as incoherent ceramic particles (carbides^[75-80], nitrides^[81,82], oxides^[83], and so on), and coherent L_{12} ^[84-89]. Among these second hardening phases, it was found that the coherent L_{12} phase can significantly improve the tensile strength of the as-printed FCC HEAs without seriously sacrificing ductility.

AM of single-phase HEAs

FCC HEAs can be well manufactured by AM methods due to their excellent workability. The defects,

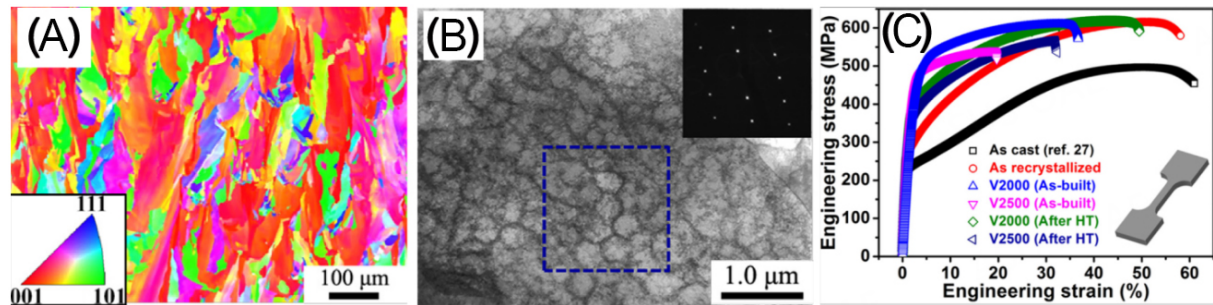


Figure 4. Hierarchical microstructure and tensile properties of FeCoCrNiMn HEA fabricated by L-PBF: (A) inverse pole figure mapping of as-printed sample along the building direction; (B) bright-field scanning transmission electron microscopy (BF-STEM) image of cellular structure with corresponding SAED pattern; (C) engineering stress-strain curves of as-printed and as-cast samples (“V2000” and “V2500” represent the scanning speed of the laser with values of 2000 and 2500 mm/s, respectively)^[59].

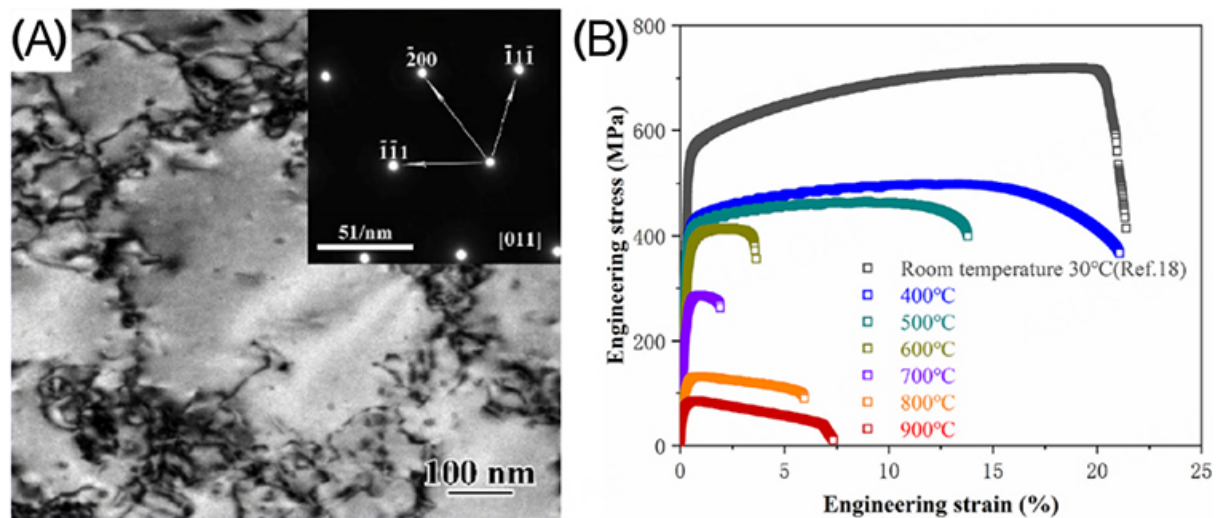


Figure 5. Microstructure and tensile properties of as-printed FeCoCrNi HEA: (A) TEM image of FeCoCrNi HEA fabricated by L-PBF showing high-density dislocation networks; (B) strain-stress curves of L-PBF-HEAs at different temperatures^[63].

microstructures and mechanical properties of as-printed FCC HEAs have been widely studied. Zhu *et al.* illustrated that a high relative density of 99.2% can be obtained by adopting suitable L-PBF parameters^[59]. In addition, due to the ultrafast cooling rate and layer-by-layer manufacturing method of the L-PBF process, the FeCoCrNiMn HEA showed hierarchical microstructure and excellent tensile properties. As illustrated in [Figure 4A](#), coarse columnar grains were formed along the building direction, while some fine cellular structures can be observed within the columnar grains [[Figure 4B](#)]. Benefiting from the hierarchical microstructure, the as-printed HEA showed superior tensile strength to the as-cast one [[Figure 4C](#)].

However, the strengths of the as-printed FCC HEAs are still insufficient and cannot satisfy some industrial applications under extreme conditions, such as structural applications at elevated temperatures. Lin *et al.* evaluated the tensile properties of FeCoCrNi HEA fabricated by L-PBF at room and elevated temperatures^[63]. As shown in [Figure 5](#), the as-printed FeCoCrNi HEA showed high-density dislocation networks, leading to relatively high tensile properties at room temperature. Some dislocations obtained sufficient activation energy at elevated temperatures to overcome the energy barrier binding them to the networks. Therefore, the dislocation networks failed to provide sufficient resistance to dislocation movement, thereby leading to a significant decrease in strength.

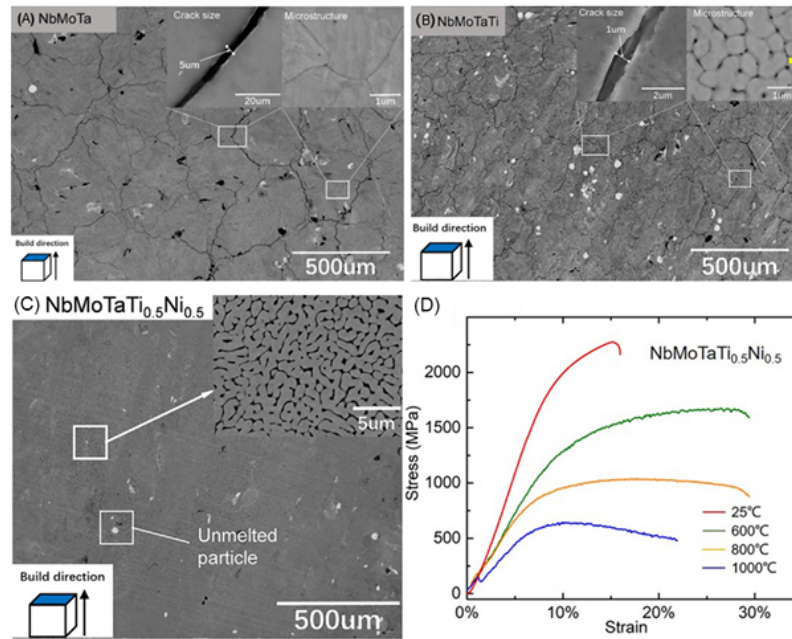


Figure 6. Microstructure and defects of refractory HEAs fabricated by L-PBF: (A) NbMoTa; (B) NbMoTaTi; (C) NbMoTaTi_{0.5}Ni_{0.5}. (D) Compressive strength of as-printed NbMoTaTi_{0.5}Ni_{0.5} at various temperatures^[67].

BCC HEAs, mostly referred to as refractory HEAs, contain refractory elements, such as V, Nb, Mo, Ta, W, Ti, Hf, and so on. Due to their sluggish diffusion rates and severe lattice distortion, refractory HEAs exhibit excellent high-temperature mechanical properties^[90]. Therefore, compared with single-phase FCC HEAs, these BCC-type refractory HEAs are considered as “the next generation of high-temperature materials,” showing a wide range of application prospects. Unfortunately, the poor workability and high cost of the raw materials make them difficult to be used at large scales. For example, Zhang *et al.* found that a NbMoTa refractory HEA fabricated by L-PBF suffers from serious grain boundary cracking due to excessive internal stress during the cooling process^[67]. As shown in Figure 6, adding Ni and Ti to the NbMoTa refractory HEA can help to suppress the crack formation and enhance its formability and high-temperature performance [Figure 6D]^[67]. The reason is mainly attributed to the formation of many extended dislocations in the grain boundary phase, which transforms the crack defects into point defects and consequently strengthens the grain boundaries. Nevertheless, limited work has been reported on the tensile properties of the refractory HEAs manufactured by L-PBF.

AM of EHEAs

As discussed above, the comprehensive properties of as-printed single-phase HEAs cannot always meet the actual requirements of the components, especially at elevated temperatures. For instance, as-printed single FCC HEAs possess excellent ductility at both room and elevated temperatures but suffer from low strength. Conversely, although refractory HEAs exhibit excellent strength at room and elevated temperatures, their ductility is greatly sacrificed. As a result, to achieve a good balance between the strength and ductility of HEAs, many researchers are now working on AM-EHEAs containing both FCC and BCC phases. The processibility, microstructure and mechanical properties of EHEAs fabricated through AM methods have been widely studied^[68,69,74,91]. Guo *et al.* illustrated that as-printed AlCoCrFeNi_{2.1} HEAs exhibited a completely eutectic structure consisting of ultrafine FCC and ordered B2 phases^[74]. The eutectic microstructure changed from a lamellar structure to a cellular structure with a decreased laser energy input, resulting in discrete tensile properties. Su *et al.* found that with increasing Al content in Al_xCrCuFeNi₂

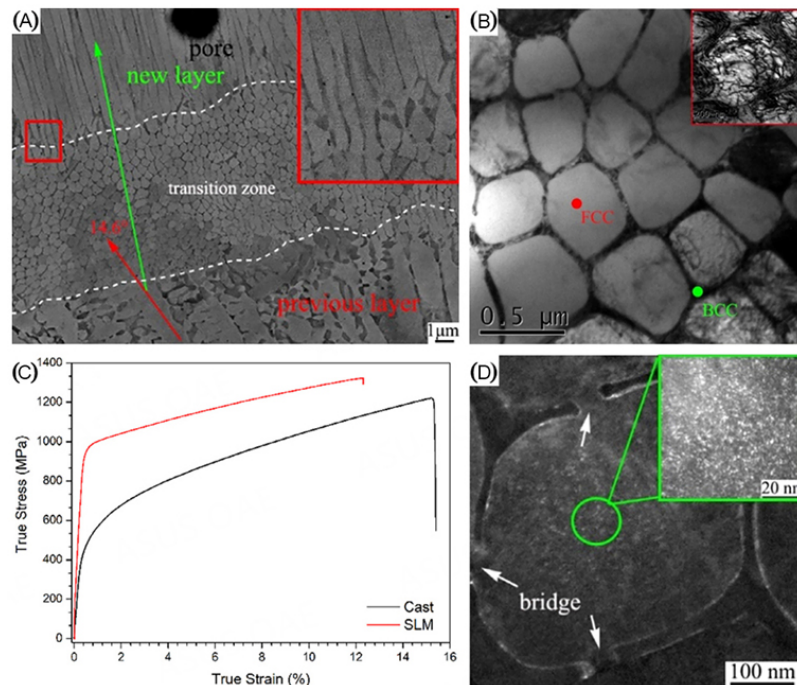


Figure 7. (A) Heterogeneous microstructure of different layers in as-printed EHEA. (B,D) Cell-like microstructure with nanosized L_{12} precipitates uniformly distributed in the FCC matrix. (C) True stress-strain curves of EHEA fabricated by cast and SLM^[69]. SLM: selective laser melting.

EHEAs, the cracking mechanisms of the as-printed samples transferred from the intergranular hot cracking induced by coarse columnar FCC grains to the transgranular cold cracking resulted from the fracture of brittle BCC grains under severe residual stress^[91]. He *et al.* fabricated a nearly fully dense and crack-free $\text{AlCoCrFeNi}_{2.1}$ EHEA by L-PBF, which showed a much superior strength to the as-cast sample^[69]. The improvement in strength can be attributed to the heterogeneous eutectic microstructure, consisting of a columnar, equiaxed and cell-like microstructure with nanosized L_{12} precipitates uniformly distributed in the FCC matrix, as illustrated in Figure 7^[69]. However, the L-PBF manufactured $\text{Ni}_{30}\text{Co}_{30}\text{Cr}_{10}\text{Fe}_{10}\text{Al}_{18}\text{W}_1\text{Mo}_1$ (at. %) EHEA showed serious softening above 650 °C, as illustrated by Yang *et al.*^[68]. Heat treatment may be needed to further improve the high-temperature mechanical properties of as-printed EHEAs by optimizing the microstructure and phase constitution.

AM of precipitation-strengthened HEAs

The tensile strength of FCC HEAs can be improved by introducing a hard ordered B2 phase. However, too much B2 phase is detrimental to the ductility and even causes severe cracking during L-PBF. Unlike the eutectic microstructure, another effective method to improve the tensile properties of as-printed FCC HEAs is to introduce strengthening particles during AM or the subsequent heat treatment. According to the literature, the strengthening phases in FCC HEAs can be generally classified into the coherent L_{12} phase and the incoherent ceramic particles, like carbides, nitrides and oxides.

Carbides can be introduced into single-phase FCC HEAs by alloying carbon to the FCC HEA powder or adding carbon to the molten pool during L-PBF, with the latter method being more flexible due to the easy control of carbon content^[75-77]. Kim *et al.* investigated the effects of carbon content on the microstructures, tensile properties and deformation mechanisms of a CoCrFeMnNi HEA fabricated by L-PBF^[77]. As shown in Figure 8, the carbide *in situ* formed during L-PBF was identified as Cr_{23}C_6 and mainly distributed along

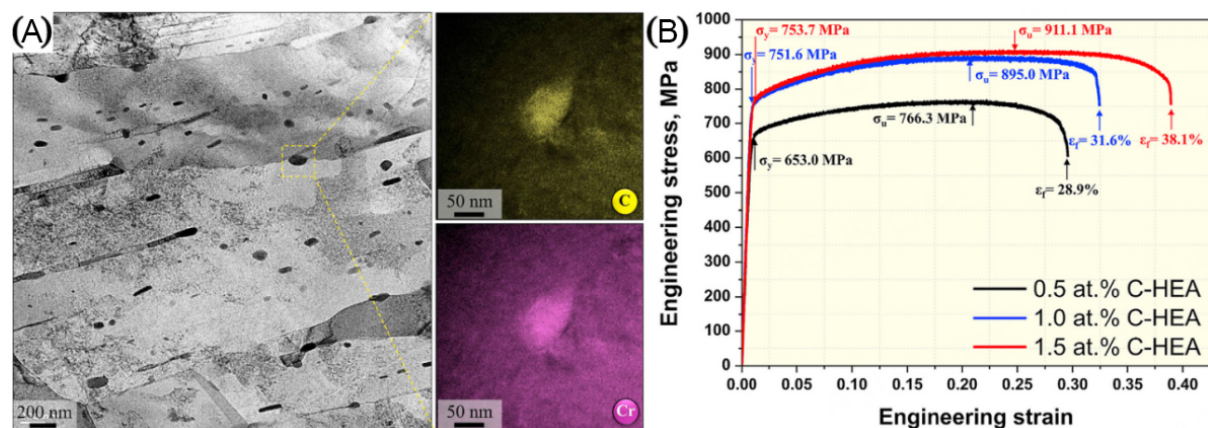


Figure 8. (A) High-angle annular dark field STEM and corresponding EELS (TEM-electron energy loss spectroscopy) mapping results to confirm nanosized carbides. (B) Representative tensile stress-strain curves for three SLM-built C-HEAs^[77]. C-HEA: C-containing HEA.

the grain boundaries. Similar phenomena were also observed in other as-printed C-containing HEAs^[75,76]. With increasing carbon content, the tensile strength and ductility were simultaneously improved. The improvement in strength can be attributed to the Cr_{23}C_6 precipitation, high back stress and easy formation of deformation twins. The high-density deformation twins and reduced pore defects are the main reasons for the ductility improvement observed.

Nitrides or N-rich structures can also be used to strengthen the FCC HEA matrix by doping TiN particles to the HEA powder through ball-milling or *in situ* formation of ordered nitrogen complexes under a nitrogen atmosphere during L-PBF. For instance, Li *et al.* fabricated a CoCrFeNiMn HEA matrix composite with nano-TiN particle reinforcements via L-PBF^[81,82]. Although the strength of the as-printed HEA composite was significantly improved due to the refined microstructures and pinning effects of TiN, the ductility of the alloy was greatly sacrificed. In addition, Zhao *et al.* found that the strength and ductility of the as-printed CoCrFeNiMn HEA were simultaneously enhanced by using a reactive $\text{N}_2 + \text{Ar}$ atmosphere during L-PBF^[92], as shown in Figure 9A. Figure 9B illustrates the schematic diagram of this L-PBF process. During fabrication, N atoms were dissolved into the molten pool to form an ordered nitrogen complex (inset of Figure 9B), which facilitated the dislocation multiplication, leading to a higher dislocation density with smaller dislocation cells. Thus, the improvement in yield strength is mainly attributed to the dislocation strengthening. In contrast, the introduction of nitrogen atoms resulted in a more heterogeneous microstructure of the matrix, leading to a higher work hardening rate and stabilizing the plastic deformation.

The oxide-dispersion-strengthening mechanism has been widely applied to traditional alloys fabricated by AM, such as steel, superalloys and Ti alloys^[93-95]. Similarly, this method can also be used to strengthen HEAs by *in situ* forming oxides during L-PBF or blending oxides with pre-alloyed powders^[83,96-98]. Chen *et al.* proposed a new method to develop an oxide-dispersion-strengthened (ODS) HEA using a L-PBF Mn-doped FeCoCrNi HEA powder^[83]. The oxide particles in the as-printed ODS HEA were proved to be MnO and Mn_2O_3 . As illustrated in Figure 10, MnO was formed by the *in situ* oxidation reaction between Mn and oxygen during the L-PBF process, while Mn_2O_3 came from the surface oxide of the Mn powder. These oxide particles hindered the dislocation movement during the tensile test, leading to a significant Orowan strengthening effect. At a high plastic strain, voids around the oxide particles were formed, reducing the tensile ductility to a certain degree. Moreover, it is interesting to find that this *in situ* formation of Mn-containing oxides can help to improve the high-cycle fatigue resistance and compressive creep

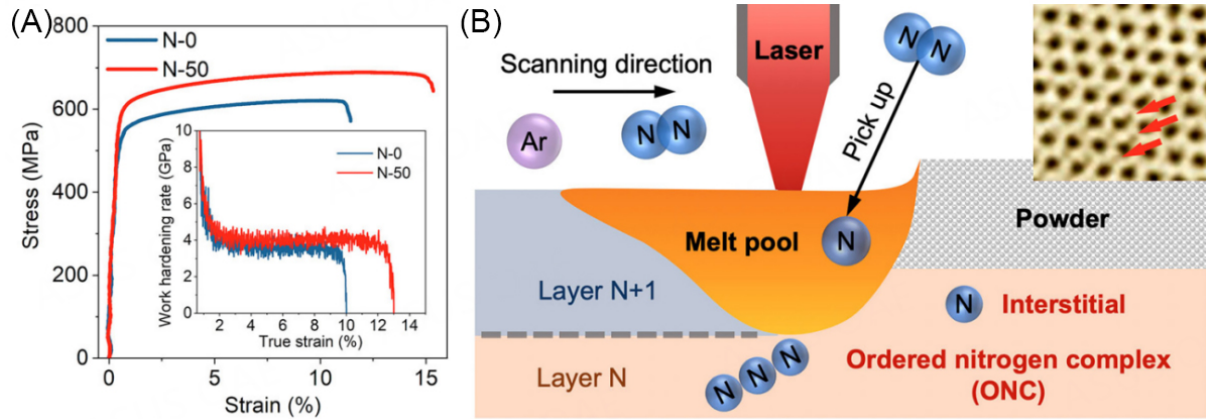


Figure 9. (A) Tensile stress-strain curve of as-printed CoCrFeMnNi HEA in different atmospheres with work hardening rate curve inserted. (B) Schematic diagram showing the *in situ* doping of nitrogen through the L-PBF process under a reactive N₂ atmosphere and the inset showing the annular bright-field STEM image of N-50 HEA^[92].

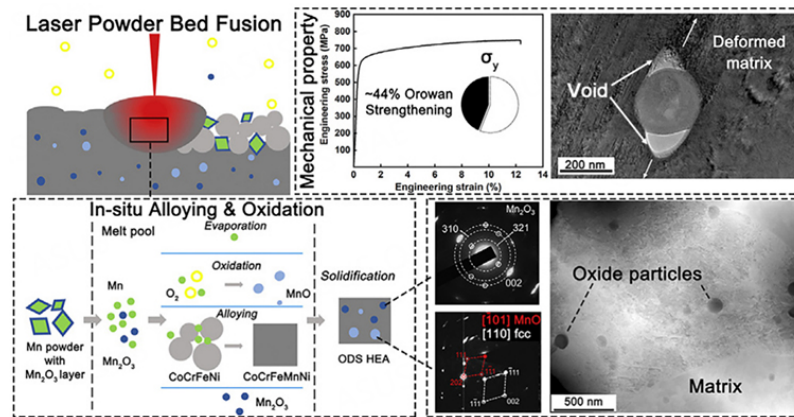


Figure 10. Microstructure and tensile properties of ODS HEA by L-PBF and schematic diagram showing oxide formation mechanism^[83]. ODS: oxide-dispersion-strengthened; HEA: high-entropy alloys.

resistance of the FeCoCrNiMn HEA fabricated by L-PBF^[96,97].

An incoherent interface is prone to cause stress concentration during deformation. Thus, the contents of the incoherent precipitations are usually controlled to a low level, which in turn limits their strengthening effects on the matrix. As discussed above, the L₁₂ precipitation coherent with the FCC HEA matrix can maintain a high content, significantly improving the tensile strength without sacrificing ductility. Mu *et al.* broke the strength-ductility trade-off by introducing high-density dislocation networks and disordered L₁₂ precipitates to the FCC HEA matrix (Fe₂₈Co_{29.5}Ni_{27.5}Al_{8.5}Ti_{6.5}, at. %) through the L-PBF and the subsequent heat treatment^[89]. Compared with the conventional L₁₂-strengthened HEA, the pre-existing high-density dislocation networks of the as-printed sample provided a fast diffusion channel for the solute atoms. Therefore, the L₁₂ precipitation was preferentially formed near the high-density dislocation networks during the aging process. Thus, an ultrahigh strength of ~1.8 GPa and a maximum elongation of ~16% were achieved for the as-printed FeCoNiAlTi HEA after aging at 780 °C for 4 h [Figure 11A]. The large ductility mainly came from the evolution of multiple stacking faults (SFs) [Figure 11B], while the ultrahigh strength was mainly derived from dislocation-precipitation synergistic strengthening [Figure 11C and D]. This work provided an efficient method to develop high-performance HEAs by simultaneously introducing

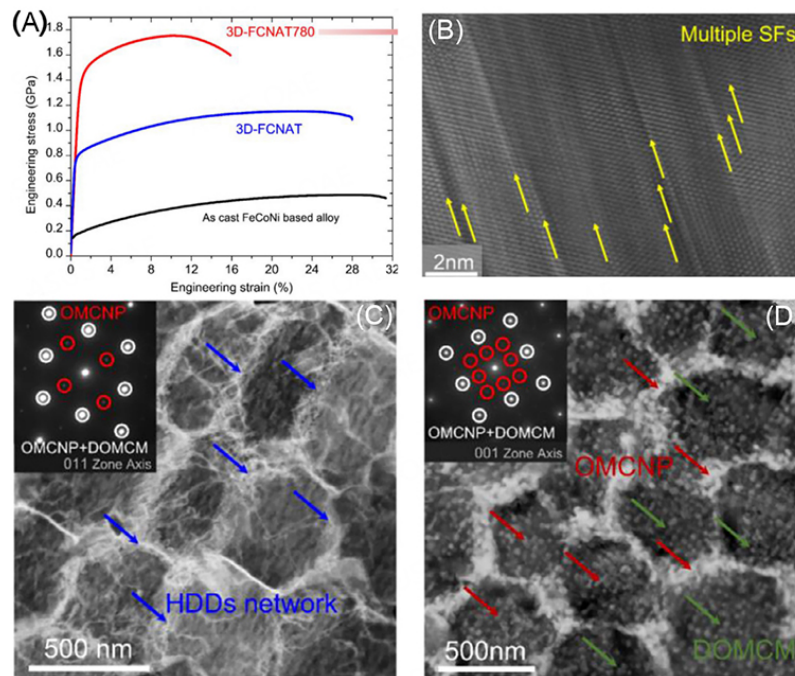


Figure 11. (A) Engineering tensile stress-strain curves of as-printed FeCoNiAlTi compared with as-cast FeCoNi based alloy. (B) HRTEM image showing multiple SFs. BF-STEM images of as-printed FeCoNiAlTi HEA after aging at 780 °C showing (C) high-density dislocations network architectures and (D) sub-grain architectures consisting of L₂-type ordered multicomponent nanoprecipitate and FCC disordered multicomponent matrix phase^[89]. SF: stacking faults; OMCNP: L₂-type ordered multicomponent nano-precipitate; DOMCM: FCC disordered multicomponent matrix; HDDs: high-density dislocations.

high-density dislocation networks and coherent particles to the matrix using the L-PBF technique and subsequent heat treatment. Similar methods have also been applied to other HEAs to improve their mechanical properties and corrosion properties, including Co_{1.5}CrFeNi_{1.5}Ti_{0.5}Mo_{0.1}, FeCoNiAlTi₇ and FeCoNiAl₃Ti₃^[85-88].

Strengthening and toughening mechanisms in AM of HEAs

The mechanical properties of HEAs from AM are usually superior to those of as-cast samples, which can be attributed to the simultaneous activation of various strengthening mechanisms, including dislocation strengthening, grain refining strengthening, solid solution strengthening, precipitation hardening and twinning/transformation-induced plasticity (TWIP/TRIP).

Dislocation strengthening is widely recognized as one of the main reasons for the enhanced yield strength of single-phase HEAs from AM. Due to the ultrafast cooling rate of L-PBF, a high-density nanosized cell structure is formed within the as-printed FeCoCrNiMn HEA^[59]. In addition, the cell walls are decorated with high-density dislocations [Figure 4B]. The cell walls act as obstacles to the dislocation motion, leading to a significant increase in dislocation density within the cell walls. Zhu *et al.*^[59] calculated the contributions of grain refinement and dislocation strengthening to the yield strength based on the following equation^[99]:

$$\sigma_y = \sigma_0 + k / \sqrt{d} + \alpha M G b \sqrt{\rho} \quad (1)$$

where σ_y is the yield strength, σ_f is the friction stress, $\Delta\sigma_{gr}$ refers to grain refinement strengthening (k is the Hall-Petch slope and d is the grain size) and $\Delta\sigma_{dis}$ refers to the dislocation strengthening (α is a constant, M is the Taylor factor of 3.06, G is the shear modulus, b is the Burgers vector of full dislocations and ρ stands for the dislocation density). This revealed that the enhanced yield strength of the as-printed FCC HEA was mainly derived from the dislocation strengthening compared with the grain refinement strengthening.

Solid solution strengthening arises from the interaction of solutes with dislocations. The different atomic sizes lead to severe lattice distortion of HEAs, which impedes the dislocation movement and leads to pronounced solid solution strengthening^[100]. Ishimoto *et al.* developed a TiNbTaZrMo bio-HEA with super yield strength by L-PBF^[101]. The ultrafast cooling rate during L-PBF promoted the formation of fine grains, suppressed the elemental segregation and realized an oversaturated solid solution. The combined effects of grain refinement and solid solution strengthening were regarded as the main reasons for the excellent strength of the TiNbTaZrMo bio-HEA fabricated by L-PBF. Zhang *et al.* systematically evaluated the factors that affect solid solution strengthening by comparing the microstructures of CoCrFeNiX_{0.4} (X = Al, Nb or Ta) fabricated by powder plasma arc AM in terms of mixed entropy, mixed enthalpy, atomic radii difference, electronegativity, valence electron concentration and melting point^[102]. Compared with Al, Ta and Nb with high melting temperatures had a more significant influence on the formation of the topologically close-packed solid solution phase, which was the main reason for the enhanced strength. Furthermore, elements with significant differences in electronegativity tended to be enriched in the second solid solution phase. Therefore, it is crucial to control multiple variables when improving the mechanical properties of HEAs by introducing a solid solution phase.

TRIP is an effective method to break the strength-ductility trade-off by providing materials with extensive work hardening ability. The TRIP effect can be triggered by reducing the phase stability. Thus, metastable HEAs were developed by tuning the stacking fault energy of the matrix phase through the selection of particular alloy chemistry. In addition to the alloy composition optimization, Agrawal *et al.* also found that the TRIP effect can be tailored through L-PBF methods^[103]. As shown in Figure 12, the as-printed metastable Fe₄₀Mn₂₀Co₂₀Cr₁₅Si₅ (at. %) HEA showed a much higher work hardening ability than the as-cast sample. Due to the thermal cycling of L-PBF, heat accumulation in the previously solidified layer occurred, which promoted the formation of a high-temperature γ (FCC) phase in that layer under an ultrafast cooling rate. Therefore, the as-printed metastable Fe₄₀Mn₂₀Co₂₀Cr₁₅Si₅ HEA showed a dual phase ($\gamma + \epsilon$) microstructure, while the as-cast sample showed an ϵ phase (HCP)-dominant microstructure [Figure 12B and C]. Upon deformation, most of the metastable γ phase was transformed into the ϵ phase [Figure 12D] under tensile stress, which contributed significantly to the work hardening ability of the as-printed sample. In addition to the TRIP effect, the TWIP effect also occurred in ϵ grains, thereby inducing the non-basal plasticity.

The strengthening mechanisms of the precipitation-strengthening HEAs fabricated by L-PBF vary with precipitate types and sample states. Due to the ultrafast cooling rate of L-PBF, the coherent precipitate, such as the L₁₂ phase, is difficult to separate from the matrix. Thus, dislocation strengthening is the main reason for the excellent strength and ductility of the as-printed HEAs containing the L₁₂-forming elements. The high-density L₁₂ phase can be introduced by subsequent aging treatment, leading to the significant precipitation strengthening effects. During deformation, both L₁₂ precipitation and high-density dislocation networks can work as effective obstacles to the dislocation motion. Thus, the high strength of the as-printed sample after aging treatment can be attributed to the synergistic strengthening mechanism of the precipitates and dislocations. The plastic deformation mode is mainly dominated by SFs, which are activated in most grains and exhibit a nano-spaced SF network, multiple SFs and Lomer-Cottrell locks. These unique microstructures provide sufficient work hardening ability to the as-printed FCC HEA^[89]. In

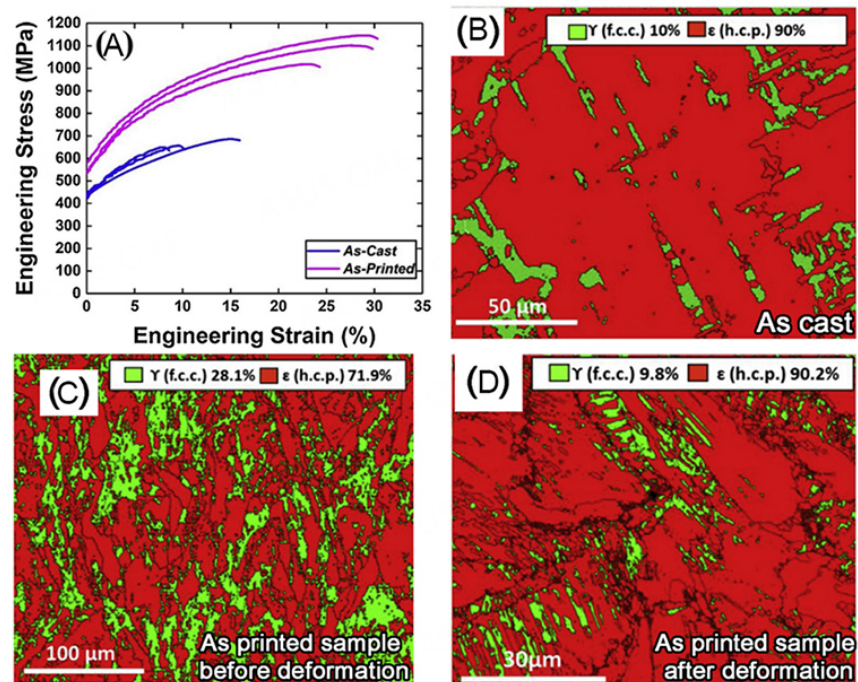


Figure 12. (A) Engineering tensile stress-strain curves of as-cast and as-printed metastable $\text{Fe}_{40}\text{Mn}_{20}\text{Co}_{20}\text{Cr}_{15}\text{Si}_5$ HEA. (B-D) Phase maps of as-cast and as-printed samples before and after deformation^[103]. FCC: face-centered-cubic; HCP: hexagonal-close-packed.

summary, due to the layer-by-layer manufacturing feature and ultrafast cooling rate of L-PBF, multiple strengthening mechanisms occur in as-printed HEAs, which can synergistically improve their mechanical properties.

MACHINE LEARNING FOR ALLOY DESIGN AND AM

The compositions of HEAs vary over a wide range, which provides an opportunity to design new alloys with enhanced properties, such as hardness, tensile property and corrosion resistance. However, it is very challenging to obtain an alloy with desired properties by a “trial and error” method due to the complexity of chemical compositions and phases. Compared with the experimental method, machine learning (ML) provides a new approach to accelerating the discovery of new materials by building the relationship between targeted properties and various materials descriptors^[104-108]. Until now, many works have been conducted to predict the possible phases in HEAs using ML algorithms, including logistic regression, random forest, decision tree, K-nearest neighbor, support vector machine and artificial neural network (ANN) approaches^[109-111]. However, how to choose suitable ML algorithms and descriptors remains a major challenge in ML due to the numerous combinations between ML models and material descriptors. Based on the genetic algorithm, Zhang proposed a framework to select the best combination of ML model and material descriptor and demonstrated its efficiency for two-phase formation problems in HEAs^[112]. Deep learning is a type of ANN algorithm generally possessing more than three hidden layers. Thus, it is an efficient data-driven modeling tool for nonlinear system dynamic modeling and identification because of its flexible structures and general approximation capabilities that can capture complex nonlinear behaviors. Thus, this method has been widely applied to predict possible phases in HEAs^[109-111,113]. For example, Lee *et al.* proposed deep learning-based ANN methods for predicting the phase structures of HEAs, i.e., solid solution, intermetallic compound, and mixed and amorphous phases. Through the Bayesian optimization for overall settings related to model architecture, training and regularization, a phase prediction model with an unprecedented accuracy of 93.17% was established^[113].

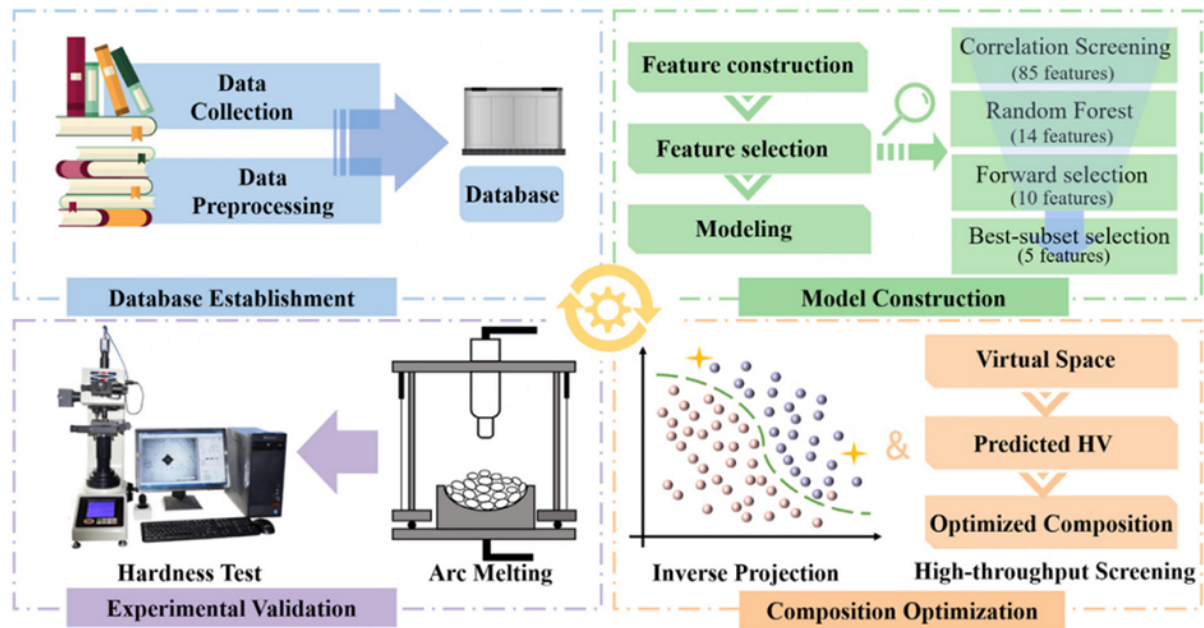


Figure 13. Diagram of ML-based alloy design system for HEAs with desired hardness^[115].

In addition to phase prediction, ML is widely used to develop new alloys with the desired properties^[114-116]. Wen *et al.* proposed a property-orientated materials design strategy to design HEAs with high hardness^[114]. ML was used to build a map between hardness and descriptors, such as chemical compositions and physicochemical properties of elements. The utility functions were employed to guide the search for Al-Co-Cr-Cu-Fe-Ni HEAs with high hardness from nearly two million possible compositions. This method developed several HEAs with hardness 10% higher than the best value in the original training dataset via only seven experiments^[114]. Yang *et al.* further proposed a new approach called ML-based alloy design system (MADS) for developing HEAs with the desired hardness^[115]. Figure 13 summarizes the overall framework of MADS, including database establishment, model construction, composition optimization and experimental validation. Through a four-step feature selection method, five key features affecting the hardness of HEAs were screened out, including the average deviation of the column, the average deviation of the specific volume, the average deviation of the atomic weight, the valence electron concentration (VEC) and the mean melting point. Among these features, VEC is the most significant variable, which positively impacts the hardness of HEAs when it is less than 7.5. Through this prediction system, one optimized sample ($\text{Co}_{18}\text{Cr}_7\text{Fe}_{35}\text{Ni}_5\text{V}_{35}$, at. %) exhibits superior hardness, which is 24.8% higher than the highest hardness in the original dataset.

In contrast, complex metallurgical behavior occurs within the micro-molten pool during L-PBF, which is greatly affected by the multiple processing parameters, such as laser power, scanning speed, hatch distance, layer thickness and scanning strategy. It is challenging to obtain suitable processing parameters through experimental methods due to the numerous combinations of these parameters. Defects, such as porosity, incomplete fusion holes and cracks, are inevitable if the processing parameters are unsuitable^[117]. It is likely that there are mature AM parameter packets provided by commercial 3D printing companies for conventional alloys, such as steel, Al alloys, Ti alloys and Ni-based superalloys. However, it is still quite difficult to obtain optimal AM parameters for newly designed alloys, such as HEAs, from experimental

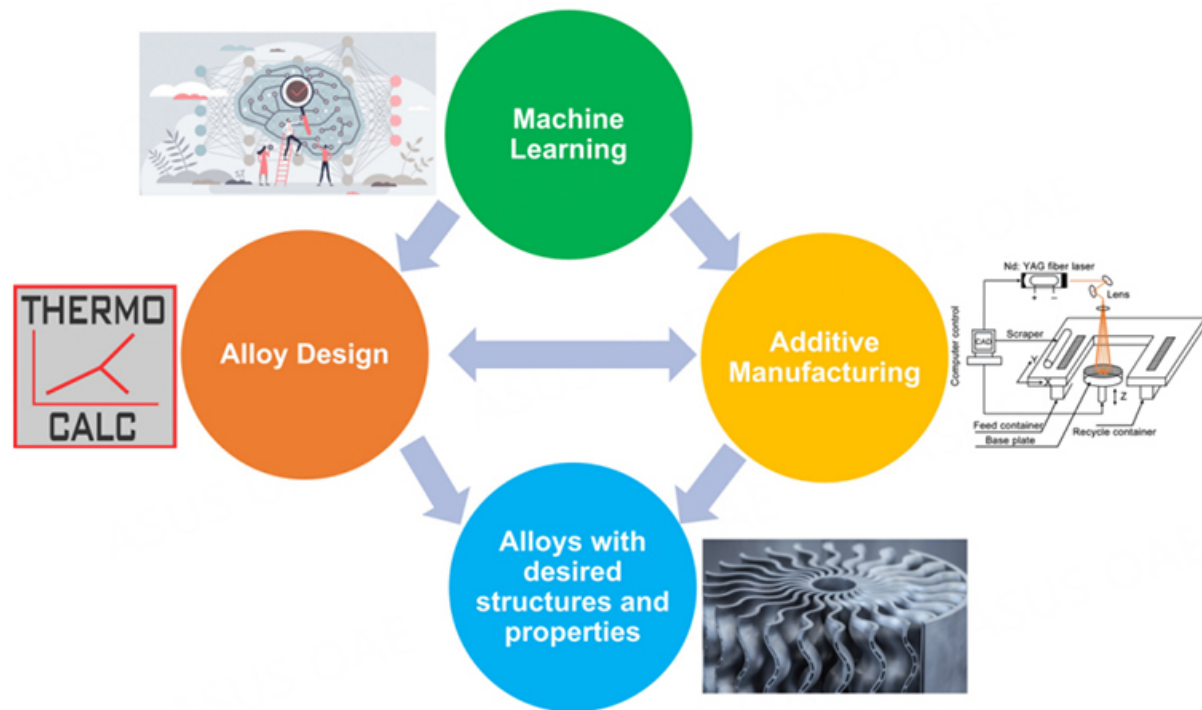


Figure 14. Relationships between ML, alloy design and AM.

methods. Zhou *et al.* developed a universal and simplified model to predict the energy density suitable for L-PBF of various metallic materials, including Ti and Ti alloys, Al alloys, Ni-based superalloys and steel, based on the relationship between energy absorption and consumption during L-PBF^[118]. The proposed model was proven to be applicable to single-phase HEAs (e.g., FeCoCrNiMn)^[118]. Compared with the calculation method, ML can describe the relationship between the descriptors and desired properties without considering the complex physical metallurgy process of AM. More importantly, AM, as a tool for high-throughput experimentation, can provide sufficient data for ML^[119]. Thus, ML has been widely used in AM for defect detection and visualization, predicting printability, optimizing processing parameters, and so on^[120-122]. This method is especially important for exploring the optimal AM processing parameters of new materials, which cannot be easily obtained through only experimental work. Figure 14 summarizes the relationships among ML, alloy design and AM. Both ML and AM can accelerate the development of new alloys. In addition, the optimal AM processing parameters for these newly developed alloys can be potentially obtained using ML. The harmonious integration of ML, alloy design and AM is expected to significantly speed up scientific advances and promote the industrial applications of these alloys.

SUMMARY AND OUTLOOK

The concept of HEAs based on multicomponent elements offers an opportunity to design attractive new alloys with desirable properties. Furthermore, AM, as a unique processing method, can maximize the capability of HEAs. In this review, we have carefully summarized the new trend in AM of multiphase HEAs and some of the applications of ML used in this aspect. The introduction of second phases to HEAs significantly improves their tensile properties. Among them, the L_2 phase, which is generally coherent with the surrounding FCC matrix, is thought to be the most effective reinforcement to improve the strength without sacrificing ductility. Different strengthening and toughening mechanisms are also reviewed for the as-printed multiphase HEAs, including dislocation strengthening, grain refining strengthening, solid

solution strengthening, precipitation hardening and TWIP/TRIP. The main obstacles to designing multiphase HEAs and obtaining optimal AM parameters lie in tedious experiments. ML would be an effective way to solve this critical problem by simplifying the relationship between the descriptor and targeted properties without considering the complex physical metallurgy process. However, there still exist some critical issues that need to be solved in the future:

Although as-printed multiphase HEAs show excellent properties at room temperature, their mechanical properties at elevated temperatures are rarely reported. Like Ni-based superalloys, HEAs undergo an embrittling behavior at intermediate temperatures of ~650-900 °C, which is known as intermediate-temperature embrittlement^[123-125]. This kind of behavior may also exist in as-printed HEAs and how to solve this key problem should be one of the focuses of future research.

Microstructure and phase stability at elevated temperatures essentially determine the working temperature range and engineering reliability of as-printed HEAs. High-density dislocation networks are thought as one of the main reasons for the enhanced properties of the as-printed sample at room temperature. How these microstructures evolve at elevated temperatures is a matter of concern. More importantly, these dislocation structures may significantly influence the resistance against high-temperature creep and oxidation, which also deserves detailed studies^[97,126].

ML is expected to provide an effective method to screen alloys with desired properties and obtain optimal AM parameters without tedious experiments. However, there are many possible ML algorithms and material descriptors, resulting in numerous possibilities for predictive results^[112]. Thus, a reasonable method is needed to rapidly select the best combination of the descriptors and ML algorithms. In contrast, many ML algorithms, especially those involving deep learning, lack interpretability and are often considered as black boxes^[127]. Sometimes, understanding the reasons behind the decision is more important than the decision that has been made. Therefore, efforts should be made regarding the interpretability of ML models to improve their efficiency and accuracy.

DECLARATIONS

Acknowledgements

The authors acknowledge members from Yang's Group for discussions towards the preparation of this work.

Authors' contributions

Proposed the review and wrote the manuscript: Zhou Y

Collated, analyzed, and organized the literature: Zhang Z, Wang D, Xiao W

Discussion of some key points in this review paper: Zhou Y, Ju J, Liu S, Xiao B

Provided supervision, acquired funding, and provided stylistic/grammatical revision on the manuscript: Yan M, Yang T

Availability of data and materials

Not applicable.

Financial support and sponsorship

This research is supported by the Shenzhen Science and Technology Program (Grant No. SGDX20210823104002016), the National Natural Science Foundation of China (No. 52101151), the Hong Kong Research Grant Council (RGC) (Grant No. CityU 21205621), the Shenzhen Science and Technology Innovation Commission (JCYJ20180504165824643).

Conflicts of interest

All authors declared that there are no conflicts of interest.

Ethical approval and consent to participate

Not applicable.

Consent for publication

Not applicable.

Copyright

© The Author(s) 2022.

REFERENCES

1. Yeh JW, Chen SK, Lin SJ et al. Nanostructured high-entropy alloys with multiple principal elements: novel alloy design concepts and outcomes. *Adv Eng Mater* 2004;6:299-303. DOI
2. Cantor B, Chang I, Knight P, Vincent A. Microstructural development in equiatomic multicomponent alloys. *Mater Sci Eng A* 2004;375:213-8. DOI
3. Ritchie RO, Zheng XR. Growing designability in structural materials. *Nat Mater* 2022;21:968-70. DOI PubMed
4. Ye Y, Wang Q, Lu J, Liu C, Yang Y. High-entropy alloy: challenges and prospects. *Mater Today* 2016;19:349-62. DOI
5. Zhao Y, Qiao J, Ma S et al. A hexagonal close-packed high-entropy alloy: the effect of entropy. *Mater Des* 2016;96:10-5. DOI
6. Yang T, Zhao YL, Tong Y, et al. Multicomponent intermetallic nanoparticles and superb mechanical behaviors of complex alloys. *Science* 2018;362:933-7. DOI PubMed
7. Lu Y, Dong Y, Guo S et al. A promising new class of high-temperature alloys: eutectic high-entropy alloys. *Sci Rep* 2014;4:1-5. DOI PubMed PMC
8. He F, Wang Z, Cheng P et al. Designing eutectic high entropy alloys of CoCrFeNiNb_x. *J Alloys Compd* 2016;656:284-9. DOI
9. Kuznetsov AV, Shaysultanov DG, Stepanov ND, Salishchev GA, Senkov ON. Tensile properties of an AlCrCuNiFeCo high-entropy alloy in as-cast and wrought conditions. *Mater Sci Eng A* 2012;533:107-18. DOI
10. Takeuchi A, Amiya K, Wada T, Yubuta K, Zhang W. High-entropy alloys with a hexagonal close-packed structure designed by equiatomic alloy strategy and binary phase diagrams. *JOM* 2014;66:1984-92. DOI
11. Yu P, Zhang L, Ning J et al. Pressure-induced phase transitions in HoDyYGdTb high-entropy alloy. *Mater Lett* 2017;196:137-40. DOI
12. Zhang Y, Zuo TT, Tang Z et al. Microstructures and properties of high-entropy alloys. *Prog Mater Sci* 2014;61:1-93. DOI
13. Guo L, Ou X, Ni S, Liu Y, Song M. Effects of carbon on the microstructures and mechanical properties of FeCoCrNiMn high entropy alloys. *Mater Sci Eng A* 2019;746:356-62. DOI
14. Cheng H, Wang H, Xie Y, Tang Q, Dai P. Controllable fabrication of a carbide-containing FeCoCrNiMn high-entropy alloy: microstructure and mechanical properties. *Mater Sci Technol* 2017;33:2032-9. DOI
15. Zheng M, Li C, Zhang X, Ye Z, Yang X, Gu J. The influence of columnar to equiaxed transition on deformation behavior of FeCoCrNiMn high entropy alloy fabricated by laser-based directed energy deposition. *Addit Manuf* 2021;37:101660. DOI
16. Gali A, George EP. Tensile properties of high-and medium-entropy alloys. *Intermetallics* 2013;39:74-8. DOI
17. Liu B, Wang J, Liu Y et al. Microstructure and mechanical properties of equimolar FeCoCrNi high entropy alloy prepared via powder extrusion. *Intermetallics* 2016;75:25-30. DOI
18. Lin D, Xu L, Han Y et al. Structure and mechanical properties of a FeCoCrNi high-entropy alloy fabricated via selective laser melting. *Intermetallics* 2020;127:106963. DOI
19. Peng Y, Jia C, Song L et al. The manufacturing process optimization and the mechanical properties of FeCoCrNi high entropy alloys fabricated by selective laser melting. *Intermetallics* 2022;145:107557. DOI
20. Lin D, Xu L, Jing H, Han Y, Zhao L, Minami F. Effects of annealing on the structure and mechanical properties of FeCoCrNi high-entropy alloy fabricated via selective laser melting. *Addit Manuf* 2020;32:101058. DOI
21. Xiong F, Fu R, Li Y, Xu B, Qi X. Influences of nitrogen alloying on microstructural evolution and tensile properties of CoCrFeMnNi high-entropy alloy treated by cold-rolling and subsequent annealing. *Mater Sci Eng A* 2020;787:139472. DOI
22. He J, Liu W, Wang H et al. Effects of Al addition on structural evolution and tensile properties of the FeCoNiCrMn high-entropy alloy system. *Acta Mater* 2014;62:105-13. DOI
23. Yan X, Guo H, Yang W et al. Al_{0.3}Cr_xFeCoNi high-entropy alloys with high corrosion resistance and good mechanical properties. *J Alloys Compd* 2021;860:158436. DOI
24. Zhang J, Qiu H, Zhu H, Xie Z. Effect of Al additions on the microstructures and tensile properties of Al_xCoCr₃Fe₃Ni high entropy alloys. *Mater Charact* 2021;175:111091. DOI
25. Jin X, Liang Y, Zhang L, Bi J, Zhou Y, Li B. Back stress strengthening dual-phase AlCoCr₂FeNi₂ high entropy alloy with outstanding

- tensile properties. *Mater Sci Eng A* 2019;745:137-43. DOI
26. Jin X, Zhou Y, Zhang L, Du X, Li B. A novel Fe₂₀Co₂₀Ni₄₁Al₁₉ eutectic high entropy alloy with excellent tensile properties. *Mater Lett* 2018;216:144-6. DOI
 27. Bhattacharjee T, Zheng R, Chong Y et al. Effect of low temperature on tensile properties of AlCoCrFeNi_{2.1} eutectic high entropy alloy. *Mater Chem Phys* 2018;210:207-12. DOI
 28. Chen X, Xie W, Zhu J et al. Influences of Ti additions on the microstructure and tensile properties of AlCoCrFeNi_{2.1} eutectic high entropy alloy. *Intermetallics* 2021;128:107024. DOI
 29. Vo TD, Tran B, Tieu AK, Wexler D, Deng G, Nguyen C. Effects of oxidation on friction and wear properties of eutectic high-entropy alloy AlCoCrFeNi_{2.1}. *Tribol Int* 2021;160:107017. DOI
 30. Yu Y, He F, Qiao Z, Wang Z, Liu W, Yang J. Effects of temperature and microstructure on the tribological properties of CoCrFeNiNb_x eutectic high entropy alloys. *J Alloys Compd* 2019;775:1376-85. DOI
 31. Wu Y, Cai Y, Wang T et al. A refractory Hf₂₅Nb₂₅Ti₂₅Zr₂₅ high-entropy alloy with excellent structural stability and tensile properties. *Mater Lett* 2014;130:277-80. DOI
 32. Lilensten L, Couzinié J-P, Bourgon J et al. Design and tensile properties of a BCC Ti-rich high-entropy alloy with transformation-induced plasticity. *Mater Res Lett* 2017;5:110-6. DOI
 33. Wang S, Wu M, Shu D, Zhu G, Wang D, Sun B. Mechanical instability and tensile properties of TiZrHfNbTa high entropy alloy at cryogenic temperatures. *Acta Mater* 2020;201:517-27. DOI
 34. Huang H, Sun Y, Cao P et al. On cooling rates dependence of microstructure and mechanical properties of refractory high-entropy alloys HfTaTiZr and HfNbTiZr. *Scr Mater* 2022;211:114506. DOI
 35. Chen Y, Xu Z, Wang M, Li Y, Wu C, Yang Y. A single-phase V_{0.5}Nb_{0.5}ZrTi refractory high-entropy alloy with outstanding tensile properties. *Mater Sci Eng A* 2020;792:139774. DOI
 36. Senkov O, Pilchak A, Semiatin S. Effect of cold deformation and annealing on the microstructure and tensile properties of a HfNbTaTiZr refractory high entropy alloy. *Metall Mater Trans A* 2018;49:2876-92. DOI
 37. Juan C-C, Tsai M-H, Tsai C-W et al. Simultaneously increasing the strength and ductility of a refractory high-entropy alloy via grain refining. *Mater Lett* 2016;184:200-3. DOI
 38. Zhao Y, Yang T, Tong Y et al. Heterogeneous precipitation behavior and stacking-fault-mediated deformation in a CoCrNi-based medium-entropy alloy. *Acta Mater* 2017;138:72-82. DOI
 39. Du X, Li W, Chang H et al. Dual heterogeneous structures lead to ultrahigh strength and uniform ductility in a Co-Cr-Ni medium-entropy alloy. *Nat Commun* 2020;11:1-7. DOI PubMed PMC
 40. Zhao Y, Yang T, Zhu J et al. Development of high-strength Co-free high-entropy alloys hardened by nanosized precipitates. *Scr Mater* 2018;148:51-5. DOI
 41. Fan L, Yang T, Zhao Y et al. Ultrahigh strength and ductility in newly developed materials with coherent nanolamellar architectures. *Nat Commun* 2020;11:1-8. DOI PubMed PMC
 42. Yang T, Zhao Y, Luan J et al. Nanoparticles-strengthened high-entropy alloys for cryogenic applications showing an exceptional strength-ductility synergy. *Scr Mater* 2019;164:30-5. DOI
 43. Zhao Y, Yang T, Li Y et al. Superior high-temperature properties and deformation-induced planar faults in a novel L₁₂-strengthened high-entropy alloy. *Acta Mater* 2020;188:517-27. DOI
 44. He F, Yang Z, Liu S et al. Strain partitioning enables excellent tensile ductility in precipitated heterogeneous high-entropy alloys with gigapascal yield strength. *Int J Plast* 2021;144:103022. DOI
 45. He J, Wang H, Huang H et al. A precipitation-hardened high-entropy alloy with outstanding tensile properties. *Acta Mater* 2016;102:187-96. DOI
 46. Wang Z, Zhou W, Fu L et al. Effect of coherent L₁₂ nanoprecipitates on the tensile behavior of a fcc-based high-entropy alloy. *Mater Sci Eng A* 2017;696:503-10. DOI
 47. Zhao Y, Li Y, Yeli G et al. Anomalous precipitate-size-dependent ductility in multicomponent high-entropy alloys with dense nanoscale precipitates. *Acta Mater* 2022;223:117480. DOI
 48. Liu W, Lu Z, He J et al. Ductile CoCrFeNiMo_x high entropy alloys strengthened by hard intermetallic phases. *Acta Mater* 2016;116:332-42. DOI
 49. Xiao B, Luan J, Zhao S et al. Achieving thermally stable nanoparticles in chemically complex alloys via controllable sluggish lattice diffusion. *Nat Commun* 2022;13:1-8. DOI PubMed PMC
 50. Anderson IE, White EM, Dehoff R. Feedstock powder processing research needs for additive manufacturing development. *Curr Opin Solid State Mater Sci* 2018;22:8-15. DOI
 51. Zhang Z, Zhou Y, Zhou S, Zhang L, Yan M. Mechanically blended Al: simple but effective approach to improving mechanical property and thermal stability of selective laser-melted Inconel 718. *Metall Mater Trans A* 2019;50:3922-36. DOI
 52. Zhang T, Huang Z, Yang T, et al. In situ design of advanced titanium alloy with concentration modulations by additive manufacturing. *Science* 2021;374:478-82. DOI PubMed
 53. Bikas H, Stavropoulos P, Chryssolouris G. Additive manufacturing methods and modelling approaches: a critical review. *Int J Adv Manuf Technol* 2016;83:389-405. DOI
 54. Singh DD, Arjula S, Reddy AR. Functionally graded materials manufactured by direct energy deposition: a review. *Mater Today: Proc* 2021;47:2450-6. DOI

55. Perrin AE, Schuh CA. Stabilized nanocrystalline alloys: the intersection of grain boundary segregation with processing science. *Annu Rev Mater Res* 2021;51:241-68. DOI
56. Zhu Y, Zhang K, Meng Z et al. Ultrastrong nanotwinned titanium alloys through additive manufacturing. *Nat Mater* 2022;21:1258-62. DOI PubMed
57. Frazier WE. Metal additive manufacturing: a review. *J Mater Eng Perform* 2014;23:1917-28. DOI
58. Li M-X, Sun Y-T, Wang C et al. Data-driven discovery of a universal indicator for metallic glass forming ability. *Nat Mater* 2022;21:165-72. DOI PubMed
59. Zhu Z, Nguyen Q, Ng F et al. Hierarchical microstructure and strengthening mechanisms of a CoCrFeNiMn high entropy alloy additively manufactured by selective laser melting. *Scr Mater* 2018;154:20-4. DOI
60. Li R, Niu P, Yuan T, Cao P, Chen C, Zhou K. Selective laser melting of an equiatomic CoCrFeMnNi high-entropy alloy: processability, non-equilibrium microstructure and mechanical property. *J Alloys Compd* 2018;746:125-34. DOI
61. Guo L, Gu J, Gan B et al. Effects of elemental segregation and scanning strategy on the mechanical properties and hot cracking of a selective laser melted FeCoCrNiMn-(N, Si) high entropy alloy. *J Alloys Compd* 2021;865:158892. DOI
62. Zhang C, Feng K, Kokawa H, Han B, Li Z. Cracking mechanism and mechanical properties of selective laser melted CoCrFeMnNi high entropy alloy using different scanning strategies. *Mater Sci Eng A* 2020;789:139672. DOI
63. Lin D, Xi X, Li X et al. High-temperature mechanical properties of FeCoCrNi high-entropy alloys fabricated via selective laser melting. *Mater Sci Eng A* 2022;832:142354. DOI
64. Brif Y, Thomas M, Todd I. The use of high-entropy alloys in additive manufacturing. *Scr Mater* 2015;99:93-6. DOI
65. Zhou P, Xiao D, Wu Z, Ou X. Al_{0.5}FeCoCrNi high entropy alloy prepared by selective laser melting with gas-atomized pre-alloy powders. *Mater Sci Eng A* 2019;739:86-9. DOI
66. Xu J, Duan R, Feng K et al. Enhanced strength and ductility of laser powder bed fused NbMoTaW refractory high-entropy alloy via carbon microalloying. *Addit Manuf Lett* 2022;3:100079. DOI
67. Zhang H, Zhao Y, Cai J et al. High-strength NbMoTaX refractory high-entropy alloy with low stacking fault energy eutectic phase via laser additive manufacturing. *Mater Des* 2021;201:109462. DOI
68. Yang F, Wang L, Wang Z et al. Ultra strong and ductile eutectic high entropy alloy fabricated by selective laser melting. *J Mater Sci Technol* 2022;106:128-32. DOI
69. He L, Wu S, Dong A et al. Selective laser melting of dense and crack-free AlCoCrFeNi_{2.1} eutectic high entropy alloy: synergizing strength and ductility. *J Mater Sci Technol* 2022;117:133-45. DOI
70. Wang S, Li Y, Zhang D, Yang Y, Manladan SM, Luo Z. Microstructure and mechanical properties of high strength AlCoCrFeNi_{2.1} eutectic high entropy alloy prepared by selective laser melting (SLM). *Mater Lett* 2022;310:131511. DOI
71. Luo S, Su Y, Wang Z. Tailored microstructures and strengthening mechanisms in an additively manufactured dual-phase high-entropy alloy via selective laser melting. *Sci China Mater* 2020;63:1279-90. DOI
72. Luo S, Zhao C, Su Y, Liu Q, Wang Z. Selective laser melting of dual phase AlCrCuFeNi_x high entropy alloys: formability, heterogeneous microstructures and deformation mechanisms. *Addit Manuf* 2020;31:100925. DOI
73. Nguyen T, Huang M, Li H, Tran V, Yang S. Microstructure and tensile properties of duplex phase Al_{0.25}FeMnNiCrCu_{0.5} high entropy alloy fabricated by laser melting deposition. *J Alloys Compd* 2021;871:159521. DOI
74. Guo Y, Su H, Zhou H et al. Unique strength-ductility balance of AlCoCrFeNi_{2.1} eutectic high entropy alloy with ultra-fine duplex microstructure prepared by selective laser melting. *J Mater Sci Technol* 2022;111:298-306. DOI
75. Zhou R, Liu Y, Liu B, Li J, Fang Q. Precipitation behavior of selective laser melted FeCoCrNiC_{0.05} high entropy alloy. *Intermetallics* 2019;106:20-5. DOI
76. Wu W, Zhou R, Wei B, Ni S, Liu Y, Song M. Nanosized precipitates and dislocation networks reinforced C-containing CoCrFeNi high-entropy alloy fabricated by selective laser melting. *Mater Charact* 2018;144:605-10. DOI
77. Kim Y-K, Yu J-H, Kim HS, Lee K-A. In-situ carbide-reinforced CoCrFeMnNi high-entropy alloy matrix nanocomposites manufactured by selective laser melting: carbon content effects on microstructure, mechanical properties, and deformation mechanism. *Compos B Eng* 2021;210:108638. DOI
78. Zhu Z, An X, Lu W et al. Selective laser melting enabling the hierarchically heterogeneous microstructure and excellent mechanical properties in an interstitial solute strengthened high entropy alloy. *Mater Res Lett* 2019;7:453-9. DOI
79. Park JM, Choe J, Kim JG et al. Superior tensile properties of 1% C-CoCrFeMnNi high-entropy alloy additively manufactured by selective laser melting. *Mater Res Lett* 2020;8:1-7. DOI
80. Chen H, Lu T, Wang Y et al. Laser additive manufacturing of nano-TiC particles reinforced CoCrFeMnNi high-entropy alloy matrix composites with high strength and ductility. *Mater Sci Eng A* 2022;833:142512. DOI
81. Li B, Zhang L, Xu Y, Liu Z, Qian B, Xuan F. Selective laser melting of CoCrFeNiMn high entropy alloy powder modified with nano-TiN particles for additive manufacturing and strength enhancement: process, particle behavior and effects. *Powder Technol* 2020;360:509-21. DOI
82. Li B, Qian B, Xu Y, Liu Z, Xuan F. Fine-structured CoCrFeNiMn high-entropy alloy matrix composite with 12 wt% TiN particle reinforcements via selective laser melting assisted additive manufacturing. *Mater. Lett.* 2019;252:88-91. DOI
83. Chen P, Yang C, Li S, Attallah MM, Yan M. In-situ alloyed, oxide-dispersion-strengthened CoCrFeMnNi high entropy alloy fabricated via laser powder bed fusion. *Mater Des* 2020;194:108966. DOI
84. Lin W-C, Chang Y-J, Hsu T-H et al. Microstructure and tensile property of a precipitation strengthened high entropy alloy processed

- by selective laser melting and post heat treatment. *Addit Manuf* 2020;36:101601. DOI
85. Fujieda T, Chen M, Shiratori H et al. Mechanical and corrosion properties of CoCrFeNiTi-based high-entropy alloy additive manufactured using selective laser melting. *Addit Manuf* 2019;25:412-20. DOI
 86. Fujieda T, Shiratori H, Kuwabara K et al. CoCrFeNiTi-based high-entropy alloy with superior tensile strength and corrosion resistance achieved by a combination of additive manufacturing using selective electron beam melting and solution treatment. *Mater Lett* 2017;189:148-51. DOI
 87. Wu Y, Zhao X, Chen Q et al. Strengthening and fracture mechanisms of a precipitation hardening high-entropy alloy fabricated by selective laser melting. *Virtual Phys Prototyp* 2022;17:451-67. DOI
 88. Yao N, Lu T, Feng K et al. Ultrastrong and ductile additively manufactured precipitation-hardening medium-entropy alloy at ambient and cryogenic temperatures. *Acta Mater* 2022;236:118142. DOI
 89. Mu Y, He L, Deng S et al. A high-entropy alloy with dislocation-precipitate skeleton for ultrastrength and ductility. *Acta Mater* 2022;232:117975. DOI
 90. Chen J, Zhou X, Wang W et al. A review on fundamental of high entropy alloys with promising high-temperature properties. *J Alloys Compd* 2018;760:15-30. DOI
 91. Su Y, Luo S, Wang Z. Microstructure evolution and cracking behaviors of additively manufactured AlxCrCuFeNi₂ high entropy alloys via selective laser melting. *J Alloys Compd* 2020;842:155823. DOI
 92. Zhao D, Yang Q, Wang D et al. Ordered nitrogen complexes overcoming strength-ductility trade-off in an additively manufactured high-entropy alloy. *Virtual Phys Prototyp* 2020;15:532-42. DOI
 93. Ghayoor M, Lee K, He Y, Chang C-h, Paul BK, Pasebani S. Selective laser melting of austenitic oxide dispersion strengthened steel: processing, microstructural evolution and strengthening mechanisms. *Mater Sci Eng A* 2020;788:139532. DOI
 94. Lee H, Jung JE, Kang D-S et al. Oxide dispersion strengthened IN718 owing to powder reuse in selective laser melting. *Mater Sci Eng A* 2022;832:142369. DOI
 95. Rittinghaus S-K, Wilms MB. Oxide dispersion strengthening of γ -TiAl by laser additive manufacturing. *J Alloys Compd* 2019;804:457-60. DOI
 96. Kim Y-K, Baek M-S, Yang S, Lee K-A. In-situ formed oxide enables extraordinary high-cycle fatigue resistance in additively manufactured CoCrFeMnNi high-entropy alloy. *Addit Manuf* 2021;38:101832. DOI
 97. Kim Y-K, Yang S, Lee K-A. Compressive creep behavior of selective laser melted CoCrFeMnNi high-entropy alloy strengthened by in-situ formation of nano-oxides. *Addit Manuf* 2020;36:101543. DOI
 98. Kim Y-K, Ahn J-E, Song Y, Choi H, Yang S, Lee K-A. Selective laser melted CrMnFeCoNi + 3 wt% Y₂O₃ high-entropy alloy matrix nanocomposite: fabrication, microstructure and nanoindentation properties. *Intermetallics* 2021;138:107319. DOI
 99. Kocks U, Mecking H. Physics and phenomenology of strain hardening: the FCC case. *Prog Mater Sci* 2003;48:171-273. DOI
 100. LaRosa CR, Shih M, Varvenne C, Ghazisaeidi M. Solid solution strengthening theories of high-entropy alloys. *Mater Charact* 2019;151:310-7. DOI
 101. Ishimoto T, Ozasa R, Nakano K et al. Development of TiNbTaZrMo bio-high entropy alloy (BioHEA) super-solid solution by selective laser melting, and its improved mechanical property and biocompatibility. *Scr Mater* 2021;194:113658. DOI
 102. Zhang Y, Chen X, Jayalakshmi S, Singh RA, Deev VB, Prusov ES. Factors determining solid solution phase formation and stability in CoCrFeNiX_{0.4} (X = Al, Nb, Ta) high entropy alloys fabricated by powder plasma arc additive manufacturing. *J Alloys Compd* 2021;857:157625. DOI
 103. Agrawal P, Thapliyal S, Nene S, Mishra R, McWilliams B, Cho K. Excellent strength-ductility synergy in metastable high entropy alloy by laser powder bed additive manufacturing. *Addit Manuf* 2020;32:101098. DOI
 104. Song X, Guo K, Lu H, Liu D, Tang F. Integrating computational materials science and materials informatics for the modeling of phase stability. *J Mater Inf* 2021;1:7. DOI
 105. Xi S, Yu J, Bao L et al. Machine learning-accelerated first-principles predictions of the stability and mechanical properties of L1₂-strengthened cobalt-based superalloys. *J Mater Inf* 2022;2:15. DOI
 106. Yang Y, Zhao L, Han C-X et al. Taking materials dynamics to new extremes using machine learning interatomic potentials. *J Mater Inf* 2021;1:10. DOI
 107. Liu Y, Wang J, Xiao B, Shu J. Accelerated development of hard high-entropy alloys with data-driven high-throughput experiments. *J Mater Inf* 2022;2:3. DOI
 108. Yu J, Xi S, Pan S et al. Machine learning-guided design and development of metallic structural materials. *J Mater Inf* 2021;1:9. DOI
 109. Huang W, Martin P, Zhuang HL. Machine-learning phase prediction of high-entropy alloys. *Acta Mater* 2019;169:225-36. DOI
PubMed PMC
 110. Krishna YV, Jaiswal UK, Rahul M. Machine learning approach to predict new multiphase high entropy alloys. *Scr Mater* 2021;197:113804. DOI
 111. Zhou Z, Zhou Y, He Q, Ding Z, Li F, Yang Y. Machine learning guided appraisal and exploration of phase design for high entropy alloys. *NPJ Comput Mater* 2019;5:1-9. DOI
 112. Zhang Y, Wen C, Wang C et al. Phase prediction in high entropy alloys with a rational selection of materials descriptors and machine learning models. *Acta Mater* 2020;185:528-39. DOI
 113. Lee SY, Byeon S, Kim HS, Jin H, Lee S. Deep learning-based phase prediction of high-entropy alloys: optimization, generation, and explanation. *Mater Des* 2021;197:109260. DOI

114. Wen C, Zhang Y, Wang C et al. Machine learning assisted design of high entropy alloys with desired property. *Acta Mater* 2019;170:109-17. [DOI](#)
115. Yang C, Ren C, Jia Y, Wang G, Li M, Lu W. A machine learning-based alloy design system to facilitate the rational design of high entropy alloys with enhanced hardness. *Acta Mater* 2022;222:117431. [DOI](#)
116. Bhandari U, Rafi MR, Zhang C, Yang S. Yield strength prediction of high-entropy alloys using machine learning. *Mater Today Commun* 2021;26:101871. [DOI](#)
117. Zhang B, Li Y, Bai Q. Defect formation mechanisms in selective laser melting: a review. *Chin J Mech Eng* 2017;30:515-27. [DOI](#)
118. Zhou Y, Zhang Z, Wang Y et al. Selective laser melting of typical metallic materials: an effective process prediction model developed by energy absorption and consumption analysis. *Addit Manuf* 2019;25:204-17. [DOI](#)
119. Xiong W. Additive manufacturing as a tool for high-throughput experimentation. *J Mater Inf* 2022;2:12. [DOI](#)
120. Westphal E, Seitz H. A machine learning method for defect detection and visualization in selective laser sintering based on convolutional neural networks. *Addit Manuf* 2021;41:101965. [DOI](#)
121. Chen Y, Wang H, Wu Y, Wang H. Predicting the printability in selective laser melting with a supervised machine learning method. *Materials* 2020;13:5063. [DOI](#) [PubMed](#) [PMC](#)
122. Park HS, Nguyen DS, Le-Hong T, Van Tran X. Machine learning-based optimization of process parameters in selective laser melting for biomedical applications. *J Intell Manuf* 2022;33:1843-58. [DOI](#)
123. Zheng L, Schmitz G, Meng Y, Chellali R, Schlesiger R. Mechanism of intermediate temperature embrittlement of Ni and Ni-based superalloys. *Crit Rev Solid State Mater Sci* 2012;37:181-214. [DOI](#)
124. Yang T, Zhao Y, Fan L et al. Control of nanoscale precipitation and elimination of intermediate-temperature embrittlement in multicomponent high-entropy alloys. *Acta Mater* 2020;189:47-59. [DOI](#)
125. Cao B, Wei D, Zhang X et al. Intermediate temperature embrittlement in a precipitation-hardened high-entropy alloy: the role of heterogeneous strain distribution and environmentally assisted intergranular damage. *Mater Today Phys* 2022;24:100653. [DOI](#)
126. Tong Z, Liu H, Jiao J, Zhou W, Yang Y, Ren X. Laser additive manufacturing of CrMnFeCoNi high entropy alloy: microstructural evolution, high-temperature oxidation behavior and mechanism. *Opt Laser Technol* 2020;130:106326. [DOI](#)
127. Zhong X, Gallagher B, Liu S, Kailkhura B, Hiszpanski A, Han T. Explainable machine learning in materials science. *NPJ Comput Mater* 2022;8:1-19. [DOI](#)